Aerodynamics of Small-Scale Vertical-Axis Wind Turbines

Ion Paraschivoiu* and Philippe Désy†
École Polytechnique de Montréal, Québec, Canada

The purpose of this work is to study the influence of various rotor parameters on the aerodynamic performance of a small-scale Darrieus wind turbine. To accomplish this, a straight-bladed Darrieus rotor was investigated using the double-multiple-streamtube model including the streamtube expansion effects through the rotor (CARDAAX computer code) and the dynamic-stall effects. The straight-bladed Darrieus turbine is, as expected, more efficient with respect to the curved-bladed rotor, but for a given solidity it operates at higher wind speeds.

Nomenclature

c	= blade chord, m
C_D, C_L, C_N	= blade airfoil section drag, lift, and normal-force coefficients, respectively
C_P	= rotor power coefficient, $\bar{T}\omega/(\frac{1}{2}\rho_\infty V_\infty^3 S)$
C_Q	= rotor torque coefficient, $\bar{T}/(\frac{1}{2}\rho_\infty V_\infty^2 SR)$
C_T	= blade airfoil section tangential-force coefficient
C_X, C_Y	= drag-force and side-force coefficients, Eqs. (24) and (25), respectively
F_{NX}^+, F_{NX}^+	= upwind and downwind blade-load coefficients normal to the tower, Eq. (8)
F_T^+, F_T^+	= upwind and downwind blade tangential-load coefficients, Eq. (9)
H	= half-height of the rotor, m
K_p	= performance coefficient, C_p/X_{EQ}^3
N	= number of blades
R	= rotor radius, m
Re_b	= blade Reynolds number, Wc/ν_∞
Re_t	= turbine Reynolds number, $\omega cR/\nu_\infty$
S	= rotor swept area, m^2
$\bar{T}$	= average rotor torque, Nm
u,u'	= upwind and downwind interference factors, Eqs. (3a) and (3c), respectively
V,V'	= upwind- and downwind-induced velocities, m/s
V_e	= equilibrium-induced velocity, m/s
V_∞	= wind velocity at the equator level, m/s
W, W'	= upwind and downwind relative inflow velocities, m/s
X_{EQ}	= tip-speed ratio at the equator, $\omega R/V_\infty$
z	= local turbine height, m
α,α'	= upwind and downwind local angles of attack, deg
α_w	= atmospheric wind-shear exponent
ζ	= nondimensional Cartesian coordinate, z/H
θ	= azimuthal angle, deg
ρ_∞	= freestream density, kg/m^3
ω	= turbine rotational speed, s^{-1}

Superscripts

$(\,)'$	= downwind conditions; no prime denotes upwind conditions
$(\bar{\ })$	= average values

Subscripts

EQ	= equatorial values
MAX,max	= maximum values
∞	= freestream conditions
∞i	= local conditions in the vertical direction

Introduction

MOST of the existing Darrieus wind turbines operating in natural conditions have been in connection with the curved blades (parabola, catenary, ideal troposkien, and Sandia shape). Some studies show that the catenary shape produces the largest maximum power coefficient, $C_{P\max}$, but the Sandia-type machine (straight-line/circular-arc shape) is better from the point of view of the performance coefficient $K_{P\max}$ and manufacture.

The straight-bladed vertical-axis wind turbines were not considered to be an interesting device due to the structural and aerodynamic disadvantages of the configuration. Recently, Migliore[1] described a protagonist's view of the straight-bladed Darrieus wind turbines and showed that many improvements can be achieved in the structural integrity and aerodynamic efficiency by utilizing moderate taper of both support arms and blades. The structural problems can be solved by limiting the operating rotational speed and using thicker and stronger sections of the strutted blades. Thus, the straight-bladed Darrieus machines might well be more economical in certain power and wind-speed regimes.

A practical model was developed a few years ago using two constant interference factors over the front and back halves of the rotor for estimating the induced velocities.[2] This so-called "double-multiple-streamtube model" (CARDAA computer code) is useful for predicting the overall aerodynamic performance and loads and for structural dynamic studies[3] of the Darrieus straight- and curved-bladed rotor. This model is capable of distinguishing between upwind and downwind blade forces; the calculations were made on the basis of the local Reynolds number and the local angle of attack.

The previous CARDAA computer code was improved by considering the variation in the upwind- and downwind-induced velocities as a function of the azimuthal angle for each streamtube.[4] This variant assumes angular streamtubes within a computation procedure based on the use of the CARDAAV computer code. The influence of the secondary effects on induced velocities, namely, the blade geometry and profile type, the rotating tower, and the presence of struts and aerodynamic spoilers, is relatively significant, especially at high tip-speed ratios.[5] The description of the CARDAA and CARDAAV computer codes is given in Ref. 6.

Recently we proposed a new variant of the double-multiple-streamtube model by considering the streamtube expansion effects on the Darrieus wind turbine. These effects, allowing a more realistic modeling of the upwind/downwind flowfield asymmetries inherent in the Darrieus rotor, were included by

Received Aug. 12, 1985; revision received Jan. 2, 1986.

*Associate Professor, Department of Mechanical Engineering. Member AIAA.

†Graduate Student, Department of Mechanical Engineering. Student Member AIAA.

using the CARDAAX computer code.[7] When the dynamic stall[8] is introduced in the model, the aerodynamic loads and performance show significant changes in the range of low tip-speed ratio, $X<3.5$.

The objective of this paper is to determine the aerodynamic loads and performance for a Darrieus straight-bladed wind turbine using the CARDAA, CARDAAV, and CARDAAX computer codes. All of these program schemes are based on the double-multiple-streamtube theory.

Double-Multiple-Streamtube Theory

In the double-multiple-streamtube model it was assumed that the vertical-axis Darrieus wind turbine could be represented by a pair of actuator disks in tandem at each level of the rotor, Fig. 1. The different induced velocities are considered at the upstream and downstream halves of the rotor swept volume. The flow through the rotor is considered to be subdivided into a large number of streamtubes. Any pressure variations along the boundaries between adjacent streamtubes are assumed to have negligible effects on momentum balances for the flow in the streamtube. Thus, the flow in each streamtube is assumed to be aerodynamically independent of that in all of the other streamtubes.

The upwind and downwind velocity components for each streamtube are considered different and the variations with height in the freestream velocity are incorporated into the model. The effects of turbulence or gustiness are neglected and only mean wind speeds are considered in this model. The ambient wind is assumed to be two-dimensional and the freestream velocity profile is given by the following relation:

$$V_{\infty i}/V_\infty = (Z_i/Z_{EQ})^{\alpha_w} \tag{1}$$

The flow in each streamtube is considered to be acted upon by two actuator disks: disk 1 being the upwind half of the surface swept by the rotor blades ($-\pi/2\le\theta\le\pi/2$) and disk 2 being the downwind half of the rotor ($\pi/2\le\theta\le 3\pi/2$). As a result of the forces exerted on the fluid by the actuator disks, its velocity changes along the streamtube. The induced velocity decreases in the axial streamtube direction so that the downwind component is less than the equilibrium-induced velocity and the latter is smaller than the upwind component,

$$V'' < V' < V_e < V < V_{\infty i} \tag{2}$$

If $V_{\infty i}$ is designed as the local ambient wind velocity we will have

$$V = uV_{\infty i} \tag{3a}$$

$$V_e = (2u-1)V_{\infty i} \tag{3b}$$

$$V' = u'V_e = u'(2u-1)V_{\infty i} \tag{3c}$$

$$V'' = (2u-1)(2u'-1)V_{\infty i} \tag{3d}$$

By applying the momentum equation to control volumes which contain the actuator disks, one can determine the drag forces on the disks and the two disk-induced velocities. The power and side-force coefficients are calculated by means of blade element analysis.

From Ref. 2, the local relative velocity for the upstream half-cycle of the straight-bladed rotor, $-\pi/2\le\theta\le\pi/2$, and the local angle of attack are given by

$$W^2 = V^2[(X-\sin\theta)^2+\cos^2\theta] \tag{4}$$

$$\alpha = \arcsin\{\cos\theta/[(X-\sin\theta)^2+\cos^2\theta]^{1/2}\} \tag{5}$$

For the downstream half-cycle of the rotor, $\pi/2\le\theta\le 3\pi/2$, the local relative velocity W' and local angle of attack α' can be expressed as a function of X' (or V') under local conditions, as in Eqs. (4) and (5).

The upwind nondimensional normal force, as a function of the azimuthal angle θ, is given by its projection in a direction normal to the tower by

$$F_{NX}(\theta) = 2(cH/S)F^+_{NX} \tag{6}$$

For the upwind half-cycle, the tangential-force coefficient is given by the relation

$$F_T(\theta) = 2(cH/S)F^+_T \tag{7}$$

where

$$F^+_{NX} = \frac{1}{2}\int_{-1}^{1}\left(\frac{W}{V_\infty}\right)^2 C_N\,d\zeta \tag{8}$$

$$F^+_T = \frac{1}{2}\int_{-1}^{1}\left(\frac{W}{V_\infty}\right)^2 C_T\,d\zeta \tag{9}$$

Similarly, for the downwind half-cycle of the rotor, the normal- and tangential-force coefficients can be calculated using Eqs. (8) and (9) where the velocities and blade-force coefficients must be replaced by those corresponding to the downstream flow conditions.

The blade-force coefficients C_N and C_T for the upwind zone can be written as

$$C_N = C_L\cos\alpha + C_D\sin\alpha \tag{10}$$

$$C_T = C_L\sin\alpha - C_D\cos\alpha \tag{11}$$

where the blade airfoil section-lift and drag coefficients, C_L and C_D, respectively, are obtained by interpolating NASA and Sandia Laboratories' test data using both the local Reynolds number and local angle of attack. The local Reynolds number is

$$Re_b = Wc/\nu_\infty \tag{12}$$

For the present applications, the airfoil data cover the angle-of-attack range between 0 and 180 deg (positive and

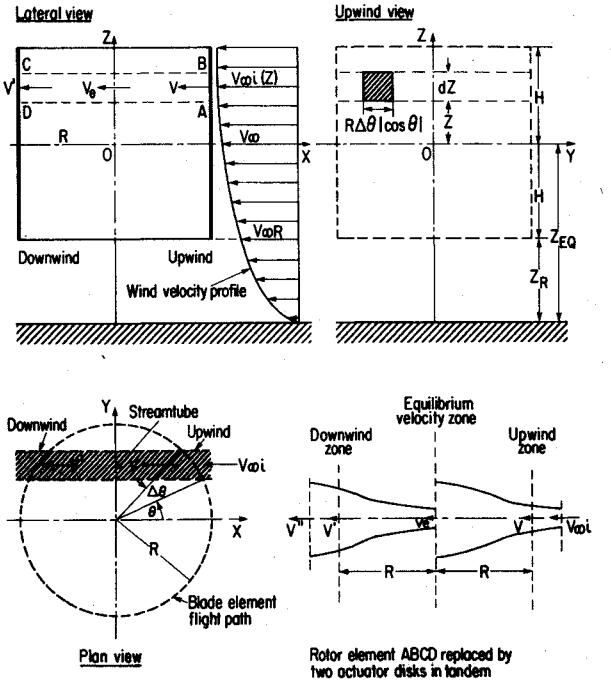

Fig. 1 Double-multiple-streamtube model.

negative values) for 11 different Reynolds numbers ($10^4 \le Re \le 10^7$). If the Reynolds number exceeds the highest value available in the stored data, the highest available Reynolds number data set is used.

This quasisteady approach is used up to an angle of attack close to the α stalling value when the dynamic stall model is considered for estimating lift and drag coefficients.

The average half-torque coefficients for the upwind and downwind zones of the straight-bladed rotor are, respectively,

$$\bar{C}_Q = \frac{NcH}{2\pi S} \int_{-\pi/2}^{\pi/2} \int_{-1}^{1} C_T \left(\frac{W}{V_\infty} \right)^2 d\zeta d\theta \tag{13}$$

and

$$\bar{C}'_Q = \frac{NcH}{2\pi S} \int_{\pi/2}^{3\pi/2} \int_{-1}^{1} C'_T \left(\frac{W'}{V_\infty} \right)^2 d\zeta d\theta \tag{14}$$

The power coefficient for the entire rotor is the weighted sum of the upwind and downwind halves of the rotor

$$C_P = (\bar{C}_Q + \bar{C}'_Q) X_{EQ} \tag{15}$$

Dynamic-Stall Model

The dynamic stall is a complex unsteady flow phenomenon which refers to the stalling behavior of an airfoil section when the angle of attack is changing rapidly with time. In the case of the Darrieus wind turbine, when the maximum operational wind speed is approached, all blade sections exceed the static stall angle, the angle of attack changes rapidly, and the whole blade works in dynamic-stall conditions. In this analysis, the Boeing-Vertol dynamic-stall model,[8] as modified by Strickland et al.[9] was used. This model assumes that the lift-curve slope and zero-lift angle remain unchanged and that dynamic effects modify only the angle of attack at which stall occurs. Thus a modified angle of attack is utilized for entering two-dimensional force-coefficient data. The modified angle of attack α_m is a function of $c\dot{\alpha}_b/(2W)$ and parameters α_b, γ, and K_1, and is given by the relation

$$\alpha_m = \alpha_b - \gamma K_1 \left(\left| \frac{c\dot{\alpha}_b}{2W} \right| \right)^{1/2} S_{\dot{\alpha}} \tag{16}$$

where W represents the relative inflow velocity, α_b is the effective blade angle of attack, γ and K_1 are empirical constants, $\dot{\alpha}_b$ represents the instantaneous rate of change of α_b, and $S_{\dot{\alpha}}$ is the sign of $\dot{\alpha}$.

The instantaneous coefficients of lift, moment, and drag are given respectively, as

$$C_L = \left(\frac{\alpha_b}{\alpha_m - \alpha_{b0}} \right) C_L(\alpha_m) \tag{17}$$

$$C_M = C_M(\alpha_m) \tag{18}$$

$$C_D = C_D(\alpha_m) \tag{19}$$

where α_{b0} is the effective blade angle of attack for zero lift. The values of γ are functions of the airfoil thickness-to-chord ratios (t/c) and the local blade Mach number. For $t/c > 0.10$ and low Mach numbers, the values of γ_L for lift stall, γ_M for moment stall, and γ_D for drag stall are

$$\gamma_L = 1.4 - 6(0.06 - t/c) \tag{20}$$

$$\gamma_M = 1 - 2.5(0.06 - t/c) \tag{21}$$

$$\gamma_D = \gamma_M \tag{22}$$

The K_1 values change with the sign of the effective angle of attack, and are calculated by

$$K_1 = 0.75 + 0.25 S_{\dot{\alpha}} \tag{23}$$

This dynamic-stall model, which was incorporated in the CARDAA, CARDAAV, and CARDAAX computer codes, is applied when the effective angle of attack is close to the static-stall value α_{SS} (when $\alpha_b > \alpha_{SS}$ or when α_b decreases after having been above the stall angle).

Drag- and Side-Force Coefficients

Assuming that the induced velocity through the rotor is constant, single streamtube methods cannot be used to estimate the side force because the local angle of attack on a blade element on the upwind face of the rotor is equal to that on the downwind face, thus canceling out the force perpendicular to the ambient wind direction (or side force). In fact, the induced velocity on the downwind side is lower than that on the upwind side. This calculation is possible with the double-multiple-streamtube model, which can predict different induced velocities and local angles of attack on the two faces of the rotor.

For a blade element of a plan area $c\,dz$, where c is the chord of the airfoil section and dz is the element height, dF_N and dF_T represent the elemental normal and tangential forces, respectively. The elemental drag and side forces become:

$$dF_X = \tfrac{1}{2}\rho_\infty W^2 c (C_N \cos\theta + C_T \sin\theta) dz \tag{24}$$

$$dF_Y = \tfrac{1}{2}\rho_\infty W^2 c (C_N \sin\theta - C_T \cos\theta) dz \tag{25}$$

for the upwind face of the rotor and, similarly, the downwind face, where C_N and C_T have different expressions according to the local angle of attack in the downwind zone of the rotor. Thus, the drag and side forces depend very much on airfoil section data such as C_N and C_T. The total average drag and side forces are obtained by integration over a full cycle and along the full length of the rotor with N blades. The average drag and side forces are normalized with respect to the wind speed at the equatorial level V_{EQ} and the swept area S of the rotor. The drag- and side-force coefficients calculated as functions of the azimuthal angle θ show that during a full cycle of the rotor the drag force keeps the same positive sign (ambient wind direction considered to be positive) while the side force changes its sign periodically (every 90 deg).

Strut Effects

The drag on the blades is the Darrieus rotor's primary source of drag force, but that on the tower and struts also causes a reduction in the overall power output. The struts are necessary to give more rigidity to the blades and to reduce the rotor stresses; moreover, they can improve the turbine response to gravitational loads by increasing the resonant frequencies, which may be significant for large vertical-axis turbines. Apart from these positive structural merits, however, the struts have an aerodynamic disadvantage in that they disturb the flow, thus causing a resistive torque as well as entailing higher costs by increasing the complexity of the rotor. For these reasons, preliminary studies should attempt to establish the criteria for using struts. There are several possible configurations for these supports.

For example, at Sandia Laboratories an experimental comparison was made between unstrutted and strutted blades on the Sandia 17-m rotor.[10] In this case, the support struts with blade sections forming an X shape from the center of the rotor become a drag device because they operate in the wake of the blade sections extracting most of the power. Thus, when two blades are without struts the 17-m rotor produces a maximum power $P_{max} = 39.3$ kW at 42.2 rpm, whereas with struts the maximum power fall to $P_{max} = 28.9$ kW (i.e., 26% of power losses).

The parasite drag due to the struts can be reduced by changing their configuration and by aerodynamically streamlining the support arms using horizontal struts. Consequently, horizontal configurations were tested for a Giromill[11] including baseline support struts made of two tubes covered with

sheet metal, a bolted-truss configuration, and a formed and welded box shape. Finally, the latter was selected as being structurally superior, since it has a high efficiency for bending and combined loads and, at the same time, the lowest drag coefficient, resulting in the lowest power loss of all three configurations.

Several studies have been undertaken to predict the effect of strut drag on the performance of the vertical-axis Giromill rotor. Thus, Moran[12] formulated a procedure for estimating drag by considering an equivalent drag coefficient acting on the blade that produces the same rotor torque as the integrated drag of the struts. Assuming the strut to be a horizontal wing of constant chord C_a, which rotates with a constant speed ω in the induced-velocity field of the rotor, the elemental force acting on a strut length dl may be expressed as follows:

$$dF_a = \tfrac{1}{2}\rho_\infty W^2 C_a C_{D0} dl \tag{26}$$

The power losses due to the struts may be calculated by integration along the strut length for the power losses corresponding to a zero-incidence drag coefficient. The effect of parasitic losses on the power coefficient is significant for high tip-speed ratios. Thus, the resistive average torque due to the horizontal strut can be written as

$$\bar{T}_a = \frac{1}{4\pi}\rho_\infty C_a \int_{-\pi/2}^{3\pi/2} \int_{r_T}^{r} W^2 C_{D0} dl\, dl\, d\theta \tag{27}$$

and the power-loss coefficient becomes

$$C_{Pa} = \omega \bar{T}_a / (\tfrac{1}{2}\rho_\infty S V_\infty^3) \tag{28}$$

However, with some simplifications, it is possible to directly approximate the coefficient of the power losses due to a strut. To do this, the tower diameter is assumed to be very small with respect to the rotor diameter ($r_T \ll r$), at high tip-speed ratios $X_{EQ} \gg 1$ and $C_{D0} = \text{const}$; in this particular case Eqs. (27) and (28) become

$$\bar{T}_a = \tfrac{1}{8}\rho C_{D0} C_a \omega^2 r_a^4 \tag{29}$$

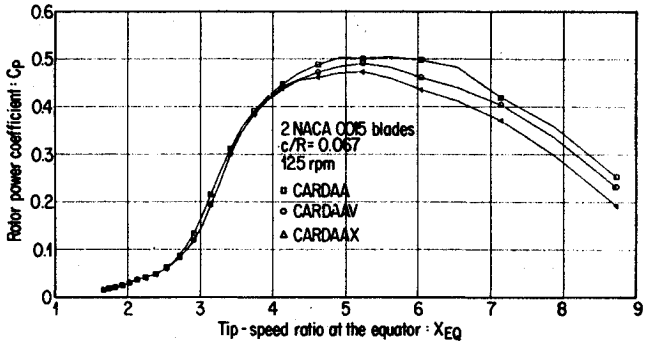

Fig. 3 Power coefficient vs tip-speed ratio. Comparison between three computer-code predictions.

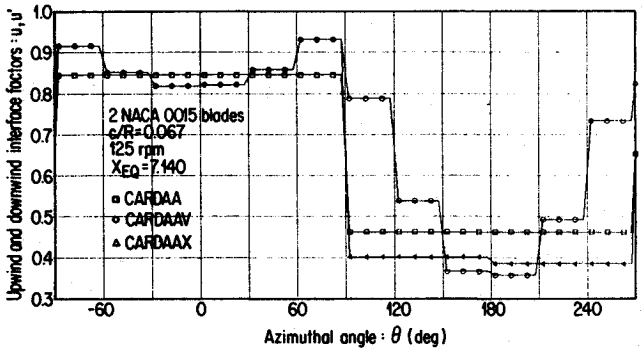

Fig. 2 Induced-velocity variation vs azimuthal angle at a tip-speed ratio of 7.14.

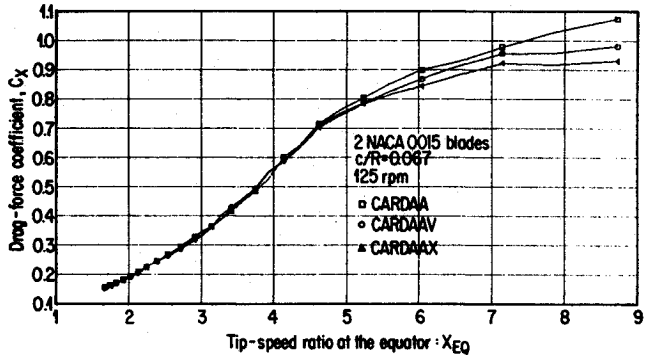

Fig. 4 Drag-force coefficient vs tip-speed ratio.

Table 1 Characteristics of rotors with straight blades and curved blades (Sandia type)

Diameter/height, β	0.984
Frontal surface of the rotor, S, m^2	13.88
Profile of the blade	NACA 0015
No. of blades	2
Distance from the ground to the equator, m	5
Speed of constant rotation, rpm	162.50
Conditions at Sandia site	
ρ_∞, kg/m^3	1.0012
ν_∞, $\times 10^{-6}$ m^2/s	17.986

Blade type	Height $2H$,m	Diameter $2R$,m	Chord length c,m	Solidity, $s = Nc\ell/S$	Reynolds no, $Re_t = \frac{\omega c R}{\nu_\infty}$, $\times 10^5$	Tip-speed ratio, $X_{EQ} = \frac{\omega R}{V_{EQ}}$	Power coefficient, C_{Pmax}
Straight:	3.756	3.696	0.153	0.083	2.68	5.000	0.421
	3.756	3.696	0.189	0.102	3.3	4.615	0.449
	3.756	3.696	0.268	0.145	4.69	4.286	0.479
Curved: (Sandia)	4.634	4.560	0.153	0.145	3.3	5.455	0.348

$$C_{Pa} = \tfrac{1}{4} C_{D0} X_{EQ}^3 (S_a/S)(r/R)^3 \qquad (30)$$

Note that the support arm power coefficient and energy loss are calculated in closed form Ref. 1.

Results and Discussion

The characteristics of three configurations of straight-bladed rotors and a frontal surface equivalent to Sandia's 5-m turbine are given in Table 1 for a turbine Reynolds number varying from $Re_t = 2.68$ to 4.69×10^5. In the case of the straight-bladed Darrieus rotor, increasing the solidity from 0.083 to 0.145 by increasing the blade chord length gives an increase in $C_{P\max}$ from 0.421 to 0.479 and a decrease in the corresponding tip-speed ratio from $X_{EQ} = 5.0$ to 4.286. At a given solidity, $s = 0.145$, the straight-bladed Darrieus turbine has a $C_{P\max} = 0.479$, while the curved-bladed Sandia 5-m turbine has a $C_{P\max} = 0.348$; this latter device operates at higher tip-speed ratios (or lower wind speeds). The tip loss corrections on the power of the straight-bladed rotor were not taken into account in these calculations.

Figure 2 presents an example of the induced-velocity profiles for a two straight-bladed rotor operating at 125 rpm for a tip-speed ratio of $X_{EQ} = 7.14$. The constant-interference factors obtained with the previous CARDAA computer code are compared to the variable-interference factors given by CARDAAV and CARDAAX. It can be seen that the constant-interference factor was underestimated on the downwind zone and that the interference factor for the streamtube with an expansion effect (CARDAAX) has the smallest values.

The power coefficient as a function of the tip-speed ratio is presented in Fig. 3. With regard to the maximum power coefficient, which occurs in all cases at the same tip-speed ratio $X_{EQ} = 5.25$, CARDAA, CARDAAV, and CARDAAX predict $C_{P\max}$ values of 0.500, 0.485, and 0.476, respectively. However, the previous publications showed that the CARDAA omputer code (with a constant-interference factor of the induced velocity) overpredicts the power-coefficient peak, while the CARDAAV and CARDAAX results are very close to the VDART3 predictions or experimental data.

Drag- and side-force coefficients on the rotor blades were calculated by Eqs. (24) and (25), respectively. Their average values over a full cycle are presented in Figs. 4 and 5 as a function of the tip-speed ratio. Slightly different values of C_X calculated with the three variants of the model appear for high tip-speed ratios. However, the side-force coefficient C_Y shows a drastic variation in a transition zone, between tip-speed ratio $X_{EQ} = 4$ and 6. Figure 6 compares the tangential-force coefficient as a function of blade position calculated by the three computer codes. There is no difference between CARDAAV and CARDAAX predictions on the upwind zone of the rotor, and the downwind zone CARDAAX gives smaller forces.

Finally, we will present the aerodynamic calculations made by CARDAAX—the more exact computer code of the double-multiple-streamtube model—on a two straight-blade (NACA 0015) Darrieus rotor having a solidity ($Nc/2R = 0.067$) operating at 125 rpm. The rotor calculated here has a height of 6 m, a diameter of 6 m, and a blade chord of 20 cm. This wind turbine is capable of producing about 10 kW of mechanical power in a wind speed of 11 m/s.

All of the following predictions are given for three tip-speed ratios: $X_{EQ} = 1.916$, 4.909, and 7.140 and the dynamic-stall effects were taken into account. Figure 7 illustrates the interference factors of the induced velocities as a function of the azimuthal angle. It can be seen that the largest difference between the upwind and downwind half-cycles of the rotor corresponds to the high tip-speed ratios when the induced velocity through the rotor is extremely nonuniform. The values of the normal-force and tangential-force coefficients as a function of the azimuthal angle were calculated by the CARDAAX computer code. These calculations show smaller forces on the downwind zone of the rotor, but the dynamic-stall effect is more significant on the tangential-force coefficient by its fluctuating values at a tip-speed ratio of 1.916. Consequently, the variation of the total aerodynamic-torque coefficient as a function of blade position is very nonuniform in the dynamic-stall operating conditions, Fig. 8.

Increasing the solidity by increasing the number of blades gives a slight increase in $C_{P\max}$ and a decrease in the corresponding tip-speed ratio. The solidity can also be changed by altering the blade chord length. The effect of increasing the

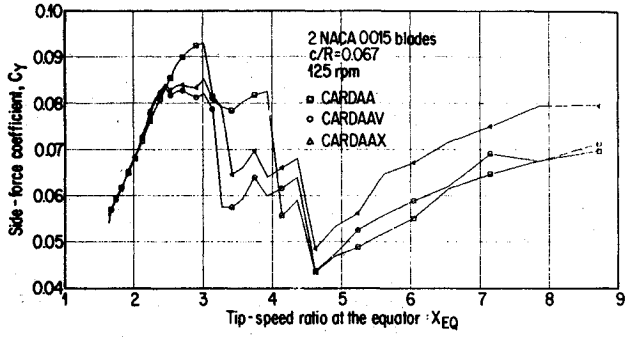

Fig. 5 Side-force coefficient vs tip-speed ratio.

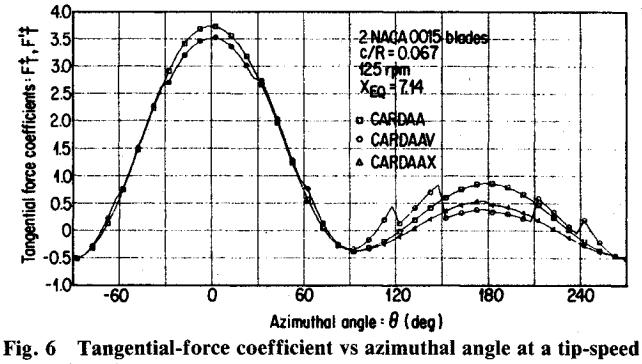

Fig. 6 Tangential-force coefficient vs azimuthal angle at a tip-speed ratio of 7.14.

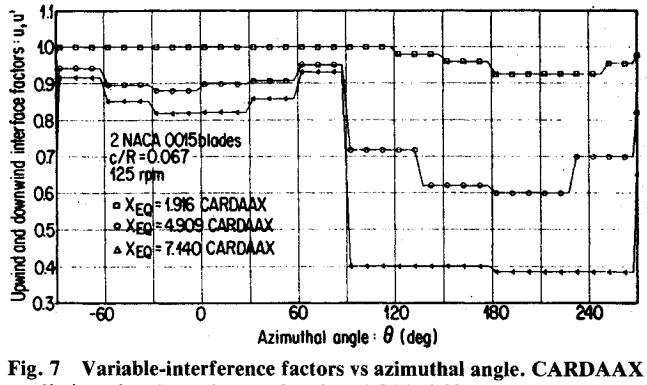

Fig. 7 Variable-interference factors vs azimuthal angle. CARDAAX predictions for three tip-speed ratios: 1.916, 4.909, and 7.140.

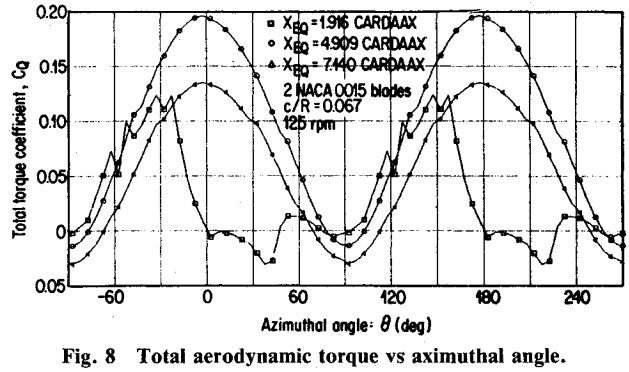

Fig. 8 Total aerodynamic torque vs aximuthal angle.

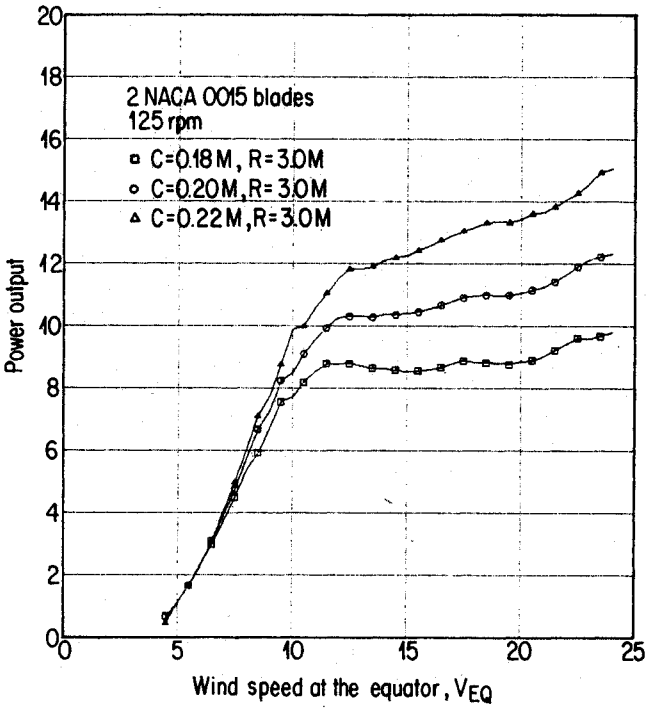

Fig. 9 Power output vs wind speed for various chord-radius ratios.

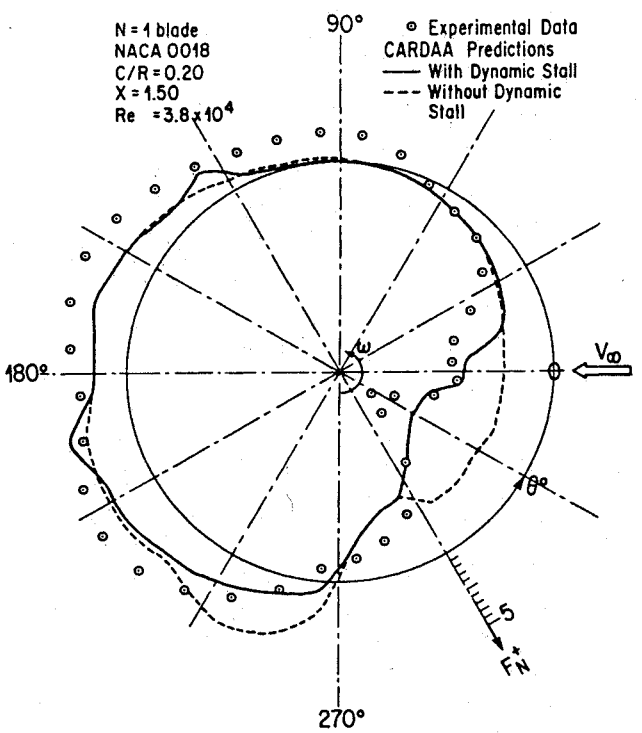

Fig. 10 Normal-force coefficient vs azimuthal angle for a single-bladed rotor at $X=1.5$.

chordlength from 0.18 to 0.22 m is shown in Fig. 9. At 125 rpm, the variations of the power output as a function of the wind speed for various chord-radius ratios are plotted in this figure. The power output increases from 8.8 to 12.5 kW at a wind speed of 20 m/s as the chordlength increases from 0.18 to 0.22 m.

Experimental Results

In order to check the validity of performance/loads models, it is essential to compare their predictions with experimental

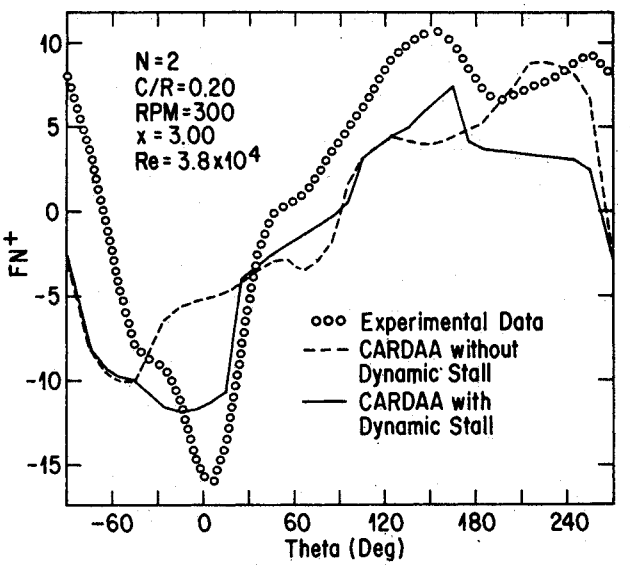

Fig. 11 Normal-force coefficient vs azimuthal angle for a two-bladed rotor at $X=3.0$.

Table 2 Experimental model characteristics

Configuration	Vertical axis
No. of blades	1 or 2
Rotor diameter, m	0.610
Blade length, m	0.610
Blade chord, m	0.061
Airfoil section	NACA 0018
Blade material	Balsa wood
Reynolds no., $\times 10^4$	3.2 and 3.8

work. Most of the existing experimental work has been in connection with the overall rotor performance and has been performed on small rotors in water[9] and wind tunnels[13] or on a real turbine operating natural conditions.[10] Some data related to the blade forces are now available but are limited to small rotors at low Reynolds numbers.[9,14]

Dynamic effects are known to be important for a Darrieus wind turbine with high chord-to-radius (c/R) ratios. These effects include added mass due to fluid inertia, unsteady wake circulation, and dynamic stall. The dynamic stall is significant at low tip-speed ratios even in rotors with small c/R values, while the other two effects take on more importance at high tip-speed ratios and for c/R values greater than 0.10.

An experimental straight-bladed Darrieus rotor with one and two blades was built and operated in a wind tunnel to measure the instantaneous aerodynamic forces. Its basic characteristics are listed in Table 2.

The values of nondimensional normal force F_N^+ calculated by CARDAA with and without dynamic-stall effects are compared with measurements in Fig. 10 for a one-bladed rotor with $c/R=0.20$ at a tip-speed ratio of 1.5. It should be noted that the dynamic-stall model incorporated into the CARDAA code shows a large improvement of the aerodynamic loads model, but the calculations are still different with respect to experimental data. In the case of the normal-instantaneous forces, the calculations with dynamic-stall effects underpredicted the experimental points for a straight-bladed rotor at a low Reynolds number of 3.8×10^4.

The effect of dynamic stall on the variation of normal- and tangential-force coefficients for a two-bladed rotor at a tip-speed ratio of $X=3.0$ is shown in Figs. 11 and 12, respectively. The aerodynamic predictions by CARDAA with and without dynamic stall[15] are compared with experiments.[14] Figure 11 represents the normal-force coefficient F_N^+ as a function of the azimuthal angle. The CARDAA prediction is improved when the Boeing-Vertol dynamic stall is incorporated into the

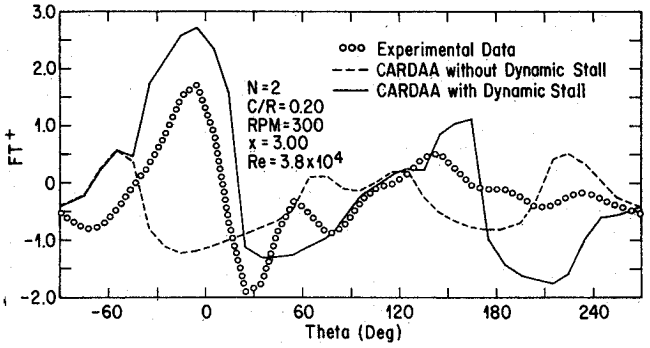

Fig. 12 Tangential-force coefficient vs azimuthal angle for a two-bladed rotor at $X=3.0$.

model. In this case, the results are much better although the experimental data are generally underpredicted. For the instantaneous tangential-force coefficient F_T^+, the CARDAA predictions with dynamic stall show good agreement for 75 deg $<\theta<$ 150 deg; the peak value of F_T^+ occurs at the same blade position in the upwind zone of the rotor, about $\theta=5$ deg, but is overpredicted by 40%. For an azimuthal angle $\theta>150$ deg, the predicted F_T^+ gives fluctuating values, with respect to experimental results, and has two peaks, in absolute values, that overestimate the measurements. This can be explained by the large solidity of the rotor ($c/R=0.20$) and by inconsistencies in the dynamic-stall model employed.

Summary and Conclusions

Planform geometries of the vertical-axis Darrieus wind turbine, studied with the double-multiple-streamtube model, include the straight cylindrical shape, a geometry which represents a major advantage over curved blades on the aerodynamic performance but is penalized by large bending moments. A straight-bladed rotor allows the size of the turbine to be reduced to an acceptable value for a given performance. This shape represents the simplest geometry and thus reduces manufacturing costs. It is recommended for low wind speed conditions and for small rotor sizes.

The stall condition, referred to as dynamic stall, produces a lift and nosedown moment, with peak values much greater than the corresponding static stall loads. The dynamic stall, while not affecting the maximum value of power coefficient, does affect the power at lower values of tip-speed ratios. However, at these tip-speed ratios, the large increase in the blade drag associated with the dynamic stall tends to stop the rotor and can cause a large increase in blade torsional loads and vibrational levels. The Boeing-Vertol dynamic-stall model was incorporated into the CARDAAX computer code and a better approximation was obtained for modeling the local aerodynamic forces and performance for a straight-bladed Darrieus rotor.

The aerodynamic analysis has also included the drag of the cross-arms, the effect of operation at low Reynolds number, and the effect of induced drag. The spanwise variation of circulation for curved-blade rotors is quite gradual and the induced drag effects can be ignored. However, for straight-bladed machines the effect of tip losses on the power is significant and corresponds in a power reduction of about 10%.

The double-multiple-streamtube model, as previously developed, does not account for the interaction of shed vorticity with the boundary vorticity on the blade. This effect is usually greatest near the blade tip, and at the very tip the flow is completely spanwise. The tips are less effective than the rest of the blade and the penalty paid is a reduced maximum-power coefficient and a large reduction in rotational speed which can increase the gearbox cost if the turbine is required to drive a generator. The wind tunnel tests were used to determine the instantaneous aerodynamic forces in the dynamic-stall conditions, and the results were compared with theoretical predictions. However, the aerodynamic loads model requires an exact dynamic-stall formulation based on the interaction between the unsteady pressure distribution and the turbulent boundary layer on the airfoil sections of the Darrieus rotor. Additional tests are necessary for a greater understanding of the dynamic effects on the Darrieus turbine. For this reason, the authors are currently working on an experimental study of dynamic stall by flow visualizations and laser-Doppler velocimetry measurements on a straight-bladed Darrieus rotor in the Institut de Mécanique Statistique de la Turbulence water tunnel.

The resulting design of a straight-bladed Darrieus turbine as analyzed in this paper can be simple, robust, and capable of operating with high efficiency at high wind velocities. This parametric study can be used for an aerodynamic optimization for a small-scale rotor design in the 1-10-kW size range for use in rural applications.

Acknowledgment

This work was supported by NSERC Grant A-4556.

References

[1]Migliore, P. G., "Straight-Bladed Darrieus Wind Turbines, a Protagonists View," *19th Intersociety Energy Conversion Engineering Conference*, San Francisco, CA, Aug. 1984, Vol. 4, p. 2326.

[2]Paraschivoiu, I., "Aerodynamic Loads and Performance of the Darrieus Rotor," *Journal of Energy*, Vol. 6, Nov.-Dec. 1982, pp. 406-412.

[3]Watson, R., "Structural Aerodynamics," Second Vertical-Axis Wind Turbine Aerodynamics Seminar, Sandia National Laboratories, Albuquerque, NM, Jan. 1982.

[4]Paraschivoiu, I. and Delclaux, F., "Double-Multiple-Streamtube Model with Recent Improvements," *Journal of Energy*, Vol. 7, May-June 1983, pp. 250-255.

[5]Paraschivoiu, I., Delclaux, F., Fraunié, P. and Béquier, C., "Aerodynamic Analysis of the Darrieus Rotor Including Secondary Effects," *Journal of Energy*, Vol. 7, Sept.-Oct. 1983, pp. 416-422.

[6]Paraschivoiu, I., "Description des logiciels CARDAA et CARDAAV pour le calcul aérodynamique des éoliennes Darrieus," Institut de Recherche d'Hydro-Québec, IREQ-8RT3010G, Jan. 1984.

[7]Paraschivoiu, I., Fraunié, P., and Béguier, C., "Streamtube Expansion Effects on the Darrieus Wind Turbine," *19th Intersociety Energy Conversion Engineering Conference*, San Francisco, CA, Aug. 1984, Vol. 4, p. 2319.

[8]Gormont, R. E., "A Mathematical Model of Unsteady Aerodynamics and Radial Flow for Application to Helicopter Rotors," Vertol Division, U.S. Army Air Mobility R&D Laboratory, Philadelphia, PA, Report on Boeing-Vertol Contract DAAJ02-71-C-0045, May 1973.

[9]Strickland, J. H., Webster, B. T., and Nguyen, T., "A Vortex Model of the Darrieus Turbine: An Analytical and Experimental Study," Sandia National Laboratories, Albuquerque, NM, SAND 79-7058, 1980.

[10]Worstell, M. H., "Measured Aerodynamics and System Performance of the 17-m Research Machine," *Proceedings of the Vertical-Axis Wind Turbine, Design Technology Seminar for Industry*, Albuquerque, NM, April 1980, pp. 233-258.

[11]Anderson, J.W., Brulle, R. V., Birchfield, E. B., and Duwe, W. D., "McDonnell 40-kW Giromill Wind System," McDonnell Aircraft Co., Rept. St. Louis, MO, RFP-3032/2 UC-60, Aug. 1979.

[12]Moran, W. A., "Giromill Wind Tunnel Test and Analysis—Vol. I: Executive Summary; Vol. II: Technical Discussion," ERDA Rept. C00/2617-4, Oct. 1977.

[13]South, P. and Rangi, R.S., "An Experimental Investigation of a 12-ft Diameter High-Speed Vertical-Axis Turbine," NRC of Canada, Ottawa, Tech. Rept. LTR-LA-166, April 1975.

[14]Vittecoq, P. and Laneville, A., "Etude en soufflerie d'un rotor de type Darrieus," Mechanical Engineering Department, University of Sherbrooke, Canada, Rept. MEC-82-2, Aug. 1982.

[15]Paraschivoiu, I., "Aerodynamic Forces on the Darrieus Rotor. Predictions and Wind Tunnel Measurments," Third Vertical-Axis Wind Turbine Aerodynamics Seminar, Sandia National Laboratories, Albuquerque, NM, March 1983.